(This is a sample cover image for this issue. The actual cover is not yet available at this time.)

Synthetic Metals 162 (2012) 1654–1664

Contents lists available at SciVerse ScienceDirect

Synthetic Metals

journal homepage: www.elsevier.com/locate/synmet

Composite films based on shape memory polyurethanes and nanostructured polyaniline or cellulose–polyaniline particles

U.M. Casado, R.M. Quintanilla, M.I. Aranguren, N.E. Marcovich*

Institute of Materials Science and Technology (INTEMA), University of Mar del Plata - National Research Council (CONICET), Av. Juan B. Justo 4302, 7600 Mar del Plata, Argentina

ARTICLE INFO

Article history:
Received 11 January 2012
Received in revised form 12 June 2012
Accepted 23 July 2012

Keywords:
Polyaniline
Nanocellulose
Composites
Shape memory polyurethanes

ABSTRACT

Conducting polyaniline (PANI) and PANI coated cellulose (PANI-NC) nanofibers doped with hydrochloric acid were synthesized by a sonochemical method and re-dispersed in methyl isobutyl ketone (MIBK) by ultrasonication. Composite films were prepared by mixing the dispersions with a segmented polyurethane (SMPu) solution in MIBK, followed by casting and solvent evaporation. PANI-NC fibers resulted more conductive than neat PANI ones and the same behavior was found for the resulting composite films, being the last ones in the range of semi-conductive polymers. As the concentration of nanofibers was maintained under 5 wt%, the thermal, mechanical and shape memory properties of the polyurethane matrix were not negatively affected or even slightly improved with the addition of nanofibers. In particular, the addition of any of the fibers led to an increase in the tensile modulus without decreasing the elongation at break, while the use of PANI ones resulted in an increase of the recovery capacity of the samples and the incorporation of PANI-NC fibers led to an increase in the recovery force. However, the transparency of the neat SMPu was lost, since even the less concentrated composite films resulted homogeneously green colored. On the other hand, no evidence of nanofiber percolation through the matrix was found.

1. Introduction

In recent years, conducting polymers have attracted much attention due to the variety of possible commercial applications [1]. Among intrinsically conducting polymers, polyaniline (PANI) is unique due to its good environmental stability, straightforward synthesis, and adjustable electrical properties [1–4]. The emeraldine base form can be easily doped by means of protic acid treatments to obtain protonated emeraldine, which is green in color and electrically conductive. However, the intractability of PANI has limited its application, especially in its pure, inherently conductive form. Processing difficulties can seriously restrict devices manufacture and function [5]. On the other hand, low-dimensional nanostructured PANI, such as nanoparticles, nanofibers and nanotubes, nanosheets and nanobelts, have received considerable attention owing to the huge number of potential applications, especially in polymeric conducting molecular wires [6], light-emitting and electronic devices [7], chemical sensors [8], and biosensors [9]. For some applications, however, conducting polymers present certain deficiencies regarding specially the mechanical performance [1]. Recently, PANI nanofibers were prepared by a series of novel template-free methods like interfacial polymerization [10], rapid mixing reaction method [11], radiolytic synthesis [12] and sonochemical synthesis [13,14]. These nanostructures demonstrate special physical and chemical properties like superior conducting and photothermal effects [15], differing from the bulk material. Furthermore, some of these nanostructures exhibit excellent dispersibility in water as shown by Jing et al. [14] and Li and Kaner [16]. Wang and Jing [4] demonstrated also that PANI nanofibers sonochemically synthesized in sulfuric acid can be easily dispersed in isobutyl ketone (MIBK) with ultrasonication to fabricate transparent conductive films based on poly(methyl methacrylate) (PMMA).

Technological uses of neat conducting polymers are not very likely because of their poor mechanical properties, which rarely meet technological expectations. However, the unique combination of electronic and mechanical properties of blends of conducting polymers with conventional polymers seems to have great promise for many applications [17].

In a two-component system comprising dispersion of a conductive polymer in a non-conductive matrix, the conductivity of the resulting blend is governed by bulk conductivity of the conducting polymer as well as the percolation behavior of the conducting polymer in the non-conductive matrix [18].

The percolation threshold depends greatly on the size of the particles as well as on the efficiency of mixing and uniformity of size [17]. In blends of doped polyaniline [17] with conventional

* Corresponding author. Tel.: +54 223 481 9669; fax: +54 223 481 0046.
E-mail address: marcovic@fi.mdp.edu.ar (N.E. Marcovich).

0379-6779/$ – see front matter © 2012 Published by Elsevier B.V.
http://dx.doi.org/10.1016/j.synthmet.2012.07.020

insulating polymers, very low (~5%) percolation thresholds were observed. It is believed that percolation is reached at a very low level since the continuous conducting polymer forms a network within the host polymer, thus forming a fine continuous conducting matrix throughout the bulk material.

The most important field of applications of conducting blends are antistatic materials [17]. Conductivities for antistatic applications need not to be high (10^{-6}–10^{-5} S/cm ranges are sufficient). Some materials using polythiophene or doped polyaniline have been already introduced for packaging of electronic items. Another very important application is electromagnetic shielding which requires higher conductivities (10^{-3}–10^{-1} S/cm, typically in anti-radar protection). Blends of conducting polymers in conventional polymers are very promising materials for this purpose. The third potentially important application of the conducting blends is their use as membranes for gas separation of high selectivity.

Chemical polymerization of conducting polymer on cellulose fiber has attracted attention recently for the manufacturing of conducting composite films and applications based on such materials [19]. Cellulose is one of the most abundant materials in nature and it naturally forms nanofibrils that can be extracted from different plants. Cellulose nanofibrils possess several advantages such as low cost, low density, non-toxicity, renewable nature, biodegradability, capability of forming stable aqueous suspensions and remarkable mechanical properties that allows improving mechanical performance of polymers at quite low fiber concentrations [20–22]. In addition to these advantages, cellulose-based nano-reinforcements are entirely organic, providing some of the mechanical improvements observed in the use of nanoclays and the added versatility of easy modification by applying well-understood cellulose chemistry [21]. Moreover, Mattoso et al. [21] prepared polyaniline coated cellulose by in situ polymerization of aniline onto "never-dried" nano cellulose fibers and demonstrated that the resulting aqueous suspensions were much more stable than PANI ones and thus, shining films with interesting electrical conductivities were obtained.

In a previous work [23], we reported the properties of composites based on a commercial shape memory polyurethane (SMPu) and PANI coated nanocellulose fibers. In that case we noticed that the changes of the material properties associated with the percolation of the coated fibrils appeared at higher concentrations than previously observed for non-modified cellulose nanofibers, which suggests that fibril agglomeration is occurring due to the PANI coating. The shape memory behavior of the composites was maintained at about the same level as that of the unfilled polyurethane only up to 4 wt% of fibrils. At higher concentrations, the rigidity of the nanofibrils as well as their interaction with the hard-segment phase and the increasing difficulty of dispersing them in the polymer collaborated to produce early breakage of the specimens when stretched at temperatures above the melting point of the soft segments [23]. In the present work, the behavior of the filler dispersion in the polymeric matrix was investigated by comparing the performance of neat PANI particles with respect to PANI coated cellulose nanofibers. Moreover, the effect of the concentration of each filler on the mechanical, thermal and dielectric properties of the resulting composites was evaluated.

2. Experimental

2.1. Preparation of cellulose nanofibers

Aqueous suspensions of cellulose crystals were prepared from commercial microcrystalline cellulose (Aldrich, Cat. No. 31,069-7) by acid hydrolysis, using an optimized procedure [20]. The microcrystalline cellulose was mixed with aqueous sulfuric acid (64 wt%) in a ratio of microcrystalline cellulose to acid of 1:8.75 g/ml. The mixture was then held at 45 °C for 0.5 h under strong stirring. The resulting suspension was diluted with an equal volume of water and dialyzed using a cellulose dialysis membrane (Spectra/Por 2, SpectrumLabs, Unitek de Argentina, molecular weight cut off = 12–14,000 Da) to pH = 5–6 to eliminate the excess of acid. The final suspension was stabilized by ultrasonic treatment (0.5 h, Elmasonic P 60H, Elma). The concentration of this suspension was determined by drying aliquots of known volume and determining the fiber weight.

2.2. Synthesis of PANI and PANI–cellulose nanofibers

PANI fibers were synthesized by the sonochemical method proposed by Jing et al. [13] and adapted with small modifications. Aniline (ANI, Carlo Erba) was doubly distilled in presence of zinc powders. Ammonium persulfate (APS. Anedra, RA-ACS) and hydrochloric acid (HCl, 36–37 wt%, Anedra, RA- ACS) were used as received. In a typical procedure, a 0.2 M solution of ANI in HCl (1 M) was prepared in a beaker and sonicated by placing the beaker in an ultrasonic cleaning bath (Elmasonic P 60H, Elma), using a power of 160 W and operated at 37 kHz. Then, 0.2 moles of APS were dissolved in 100 ml HCl (1 M) and dropwise added to the ANI containing beaker, which was kept at 25 °C during the 4 h of reaction. After that, the acid suspension was dialyzed using the membrane already described until the dialyzed water became colorless. PANI was doped in HCl (1 M, ~2 g PANI in 50 ml HCl solution) for 3 h with magnetic stirring. Finally, PANI was separated from the HCl solution by ultra-centrifugation (20 min at 12,000 rpm), washed once with distilled water and freeze-dried to yield a green powder.

The same procedure was used to synthesize PANI coated nanocellulose (PANI-NC) fibers, but in this case the nanocellulose fiber suspension (1 g/L) was previously dispersed in the ANI solution by ultrasonication. A ratio of 9.3 g ANI/g nanocellulose particles was used during synthesis.

2.3. Preparation of composite films

Composite films were prepared by suspension casting. The thermoplastic Pu (IROGRAN A60 E4902, Hunstman) was first dissolved in methyl isobutyl ketone (MIBK, Dorwill, PA) at 5 wt% and 60 °C by mild mechanical agitation (200 rpm) for 3 days. Simultaneously, PANI-MIBK and PANI-NC-MIBK suspensions at 1 wt% were prepared by ultrasonication during 2 h. The polymer solution and a selected volume of each suspension were mixed by magnetic stirring during 12 h at 95 °C. Partial evaporation of the MIBK solvent took place during this step. Then, the mixtures were sonicated during 30 min and cast onto glass plates. After 12 h drying at 65 °C in a convective oven, films of 0.4–0.5 mm thickness and containing up to 5 wt% of PANI or PANI-NC fibers were obtained.

2.4. Characterization techniques

2.4.1. Fourier transform infrared spectroscopy (FTIR)

FTIR spectra of neat SMPu, PANI and PANI-NC composites were recorded using a ThermoScientific Nicolet 6700 FTIR spectrometer in ATR mode at 32 scans with a resolution of 4 cm^{-1}.

2.4.2. UV–visible spectroscopy (UV–Vis)

UV–visible spectrum of solutions/suspensions of SMPu, PANI and PANI-NC fibers and composite samples containing 10 wt% fibers in MIBK, in the wave length range 300–1000 nm were obtained using an Agilent UV–Vis spectrometer, model 8453. Solutions and suspensions were prepared at the concentration of 0.4 g/L.

2.4.3. X ray diffraction (XRD)

XRD patterns were recorded between 2 and 60°, with a scanning rate of 1°/min by using a PANalytical X'Pert Pro diffractometer equipped with Cu Kα radiation source (λ = 0.1546 nm), operating at 40 kV and 40 mA as the applied voltage and current, respectively.

2.4.4. Atomic force microscopy (AFM)

The morphology of cellulose nanofibers was investigated using an atomic force microscope (AFM, 5500 SPM, Agilent Technologies). Specimens were prepared by depositing a drop of a very diluted NC dispersion in water onto a mica waffle, followed by spreading with nitrogen flow and finally drying at room conditions.

2.4.5. Field emission scanning electron microscopy (FESEM)

The surface morphology of PANI and PANI-NC fibers films was investigated using a field emission scanning electron microscope (Zeiss, model Leo 982 Gemini) at 3 kV. Sample specimens were prepared by depositing a very diluted drop of filler suspension in water onto a FTO glass, followed by spreading with nitrogen flow and finally drying at room conditions.

2.4.6. Scanning electron microscopy (SEM)

The morphology of PANI and PANI-NC composite films was investigated using a scanning electron microscope (JEOL, model JSM-6460LV) at 10 kV after gold coating the samples. The cross-sectional fracture surfaces of the composite films were obtained by breaking the samples after being frozen in liquid nitrogen.

2.4.7. Differential scanning calorimetry (DSC)

The thermal response of PANI, PANI-NC and composite samples was registered in the temperature range −60 to 100 °C (Perkin Elmer, Pyris 1) at a heating rate of 10 °C/min under nitrogen atmosphere.

2.4.8. Dynamic mechanical analysis (DMA)

Dynamic mechanical measurements were performed for the neat polyurethane matrix and composite films, using a rheometer (Anton Paar, Physica MCR 301) in film tension mode at 1 Hz, in the temperature range −65 to 130 °C, at a heating rate of 5 °C/min. The dimensions of the samples were 60 mm × 5 mm × 0.5 mm. The samples were subjected to a cyclic strain of 1%, being this value sufficiently small to assure that the mechanical response of the specimen was within the linear viscoelastic range. The set up was used to determine the storage modulus E', the loss modulus E'' and the ratio of these two parameters, $\tan\delta = E''/E'$.

2.4.9. Tensile tests

Tensile tests were performed at room temperature (20 ± 2° C) using an Instron Universal Testing Machine model 8501. The specimens were cut according to the ASTM D1708-93 (ASTM, 1993), in dumb-bell geometry. The length of the test specimens between clamps was 20 mm. Crosshead speed was set at 10 mm/min. The ultimate strength (σ_b), elongation at break (ε_b) and elastic modulus (E) were calculated as described in ASTM D638-94b (ASTM, 1994). At least five replicates of each sample were tested, and the average results were reported.

2.4.10. Thermal cyclic tests

Tensile cyclic tests were performed on microtensile specimens of 5 mm × 25 mm × 0.5 mm (rectangular bars) using a universal testing machine equipped with a heating chamber (INSTRON 8501). Samples were first conditioned at room temperature (20 ± 2 °C) for 10 min and subsequently elongated to 100% of the original length, at 20 mm/min cross-head speed. Then, the samples were cooled down to −50 °C by using a freezing spray (Electroquímica Delta, Argentine) and unloaded to zero loads. Finally, the specimens underwent the recovery process by heating for 10 min at room temperature, maintaining the load equal to zero. The strain maintained after unloading, and the residual strain of each cycle were used to calculate the fixity (R_f) and recovery (R_r) ratios from these tests, as indicated in the following equations:

$$R_f = 100 \times \frac{\varepsilon_u}{\varepsilon_m} \quad (1)$$

$$R_r = 100 \times \frac{\varepsilon_m - \varepsilon_p}{\varepsilon_m} \quad (2)$$

where ε_m is the maximum strain in the cycle (100%), ε_u is the residual strain after unloading at −50 °C and ε_p is the residual strain after recovery. The recovery stress (Fr), defined as the maximum stress developed by the sample during heating, was also recorded.

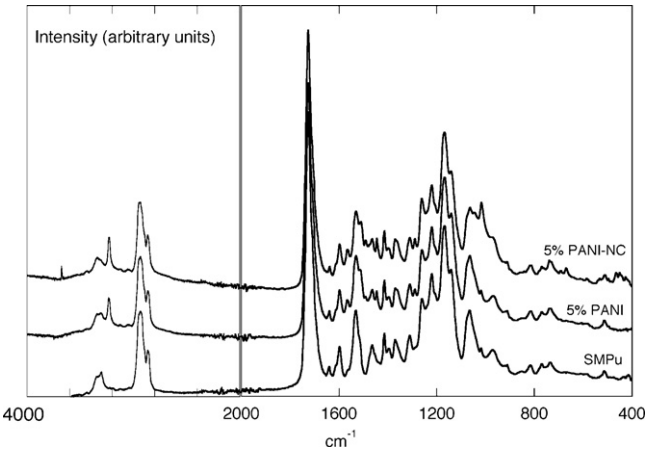

Fig. 1. FTIR spectra of neat SMPu, 5% PANI and 5% PANI-NC composites.

2.4.11. Dielectric properties

The dielectric behavior of composite films was evaluated at 15 °C, using a HIOKI-3522-50 LCR Hi-Tester for high frequency measurements and a HIOKI-3535 Hi-Tester for low frequency determinations. A voltage of 1 V was applied on disc shaped specimens of 3.14×10^{-4} m^2. The dielectric response of PANI and PANI-NC nanofibers was measured on pressed pellets (10 mm in diameter and 1.5 mm in thickness) using the same equipments. Dielectric permittivity (ε'), dielectric loss factor (ε'') and ac conductivity of the different samples were calculated from the capacitance in parallel (C_p) and loss tangent (D) values obtained from the tests.

3. Results and discussion

3.1. Physical, thermal and thermo-mechanical characterization

The commercial polymeric matrix selected for this work is an unplasticized, soft polyester based thermoplastic polyurethane. According to the producers, it has exceptional resiliency, high elastic recovery and elongation. It can be processed by extrusion and injection molding, but it also can be solvated for dip molding and cast film processing, being the last one the technique selected to prepared composite films with nanoparticles adequately dispersed. In fact, the MIBK was selected as the Pu solvent because it led to a stable suspension of well-dispersed nanoparticles after only 2 h sonication.

Fig. 1 shows the FTIR spectrum of the neat SMPu together with those corresponding to composites containing 5 wt% of nanoparticles. The neat matrix is a thermoplastic polyurethane–urea copolymer, as revealed by the broad N—H stretch peaks centered on 3330 cm^{-1}, indicative of hydrogen-bonded urethane and urea groups [24,25], while the smaller peak present at 3450 cm^{-1} is

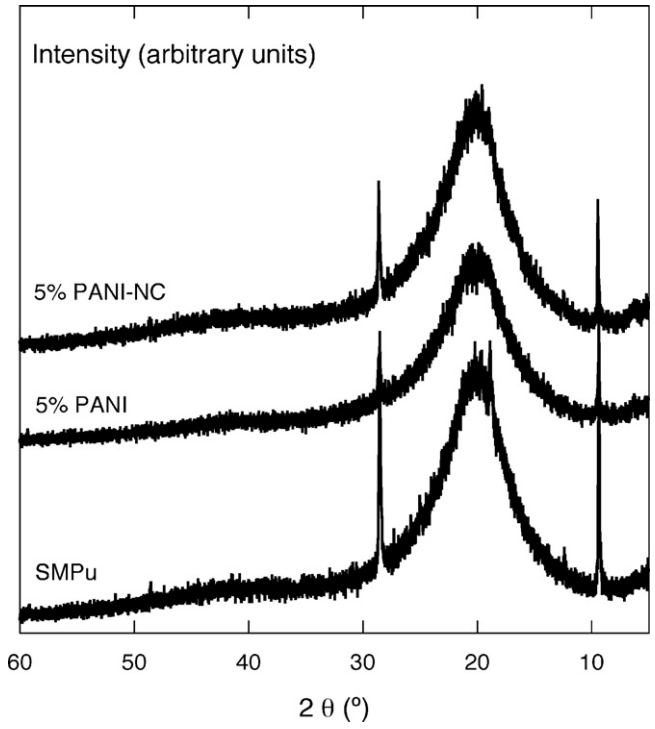

Fig. 2. X-ray diffraction patterns of neat SMPu, 5% PANI and 5% PANI-NC composites.

consistent with non hydrogen-bonded urea and urethane N—H groups [24]. The peak at 1728 cm^{-1} represents the non-hydrogen bonded carbonyl stretch [26,27] and is predominantly associated with carbonyl group in the polyester soft block, while the much weaker shoulder at 1710 cm^{-1} indicates marginal amounts of weakly or disordered hydrogen-bonded urea groups. The intensity of the band at 1600 cm^{-1} is attributed to the C=C stretching of aromatic groups [24]. Interestingly, there is no peak at 1685 cm^{-1} in the neat polyurethane indicating that there is no formation of well ordered and strongly hydrogen bonded urethane groups in the polymer [27]. This prevents the formation of a microphase-separated morphology in the solid state for SMPu and results in a polymer with no significant mechanical strength [27]. Finally, the small peak at 1640 cm^{-1} in the spectra of neat SMPu is consistent with the carbonyl stretch resonance of urea groups in a bidentate hydrogen-bonded array [27,28].

On the other hand, the spectra of the composite samples reveal clearly that PANI inclusions are in the emeraldine base form, as can be corroborated from the peak at 3228 cm^{-1} that corresponds to the overlapping of the stretching signal of the C—H groups, the deformation of benzenoid structure and to the stretching vibration of the N—H bonds [29]. Other characteristic PANI peaks are also noticed, such as those appearing at 1566, 1511, 1441 and 1288 cm^{-1} corresponding to the C=N stretching of the quinoid structure [23,30], the C=C stretching of the benzenoid ring [30], to the skeletal C=C stretching vibration of the p-substituted benzenoid ring and to the stretching vibration of $C-N^+$ for conducting PANI associated to the oxidation or protonation states [29,31]. No additional peaks that can be attributed exclusively to the cellulose are noticed in spectrum of the PANI-NC reinforced sample due to several reasons: (i) both the SMPu and the cellulose fibers are organic in nature and shear various characteristic peaks, (ii) the low concentration of cellulose in the composite sample (only 0.56 wt%) and (iii) the fact that cellulose fibers are expected to be completely coated by PANI.

WAXS measurements were performed to investigate the underlying microstructure of the SMPu as affected by the addition of conductive particles, as shown in Fig. 2. The pattern produced

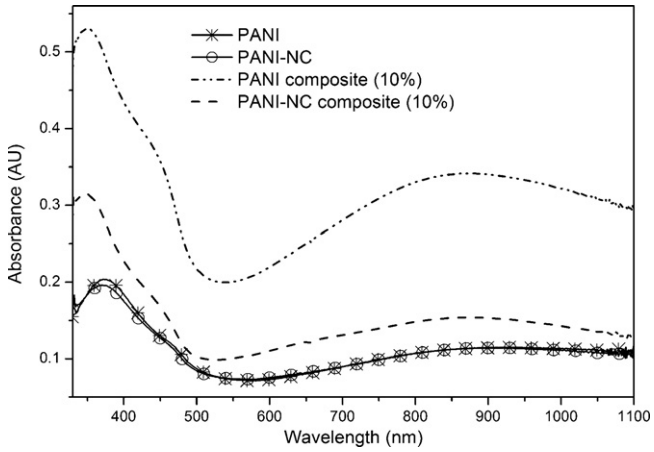

Fig. 3. UV–Vis absorption spectra of solutions/dispersions (10 wt% in MIBK) of PANI, PANI-NC and composites containing 10% of PANI or 10% PANI-NC.

by neat SMPu exhibits a nearly symmetrical diffuse maximum at $2\theta = 20.2^\circ$, indicative of short-range (translational) ordering in the arrangement of chain fragments [32,33]. Neat polymer also exhibits two weak peaks at $2\theta = 28.5^\circ$ and 9.4°, which arise from crystalline phases. The diffraction peak at $2\theta = 9.4^\circ$ can be related to the hard segment crystalline phase according to Nunes et al. [34] and/or to the spacing between the hydrogen-bonded urea groups (4.6 Å) according to Versteegen et al. [35], while the one appearing at $2\theta = 28.5^\circ$ can be attributed to soft segment crystalline phase [33]. However, the degree of crystallinity of the unfilled SMPu, taken as the area ratio of all the crystalline peaks to that of total scattering, is quite low (4%), while the corresponding crystallinity of the composites is only about 1%. This reduction in the amount of crystalline phase of the SMPu with the addition of conductive fillers indicates that important interactions between nanoparticles and matrix were developed.

The UV–Vis absorption spectra of PANI, PANI-NC and composites prepared by the dissolution/dispersion of 10 wt% sample in MIBK are shown in Fig. 3. These spectra show that PANI and PANI-NC fibers, as well as the composites exhibit a strong absorption in the same region that the unfilled polymer (280–400 nm), but they also absorbs at 850 nm, which is the dopant-induced bipolaronic transition region. This indicates that the doped state of PANI remains intact even after dissolution in organic solvents without any leaching out of the dopant [36]. This fact is also confirmed by the absence of the peak at 620 nm, characteristic of excitonic transition of the quinoid structure [41]. However, a blue shift of the polar transition band from 890 to 854 nm was observed when PANI and PANI-NC fibers were incorporated to the SMPu matrix (notice also that the neat polymeric matrix has no absorption bands in this range). In fact, the bands at 890 nm detected from the fiber dispersions have a very poor defined maxima and could be considered as broad cationic radical polaron bands or so-called free carrier tails that appear starting from 890 nm and extended to infrared region [37–40]. According to Laska [41] the presence of a narrow band in this zone proves a coil conformation of the PANI polymer chain, while band extended toward near infrared region determines an expanded conformation. Expanding coil makes it possible for the molecule to become coplanar, which allows the p-electrons to delocalize easily. The delocalization is responsible for the creation of the polaron structure of polyaniline and thus, leads to a significant increase of conductivity [41]. According to this reasoning, composite samples should be less conducting that neat fibers.

The thermoplastic Pu presents a low temperature glass transition (T_g) at −45 °C, as determined by DSC measurements, and varies in about ±0.5 °C (i.e. −44.5 to −45.5 °C) for the case of composite

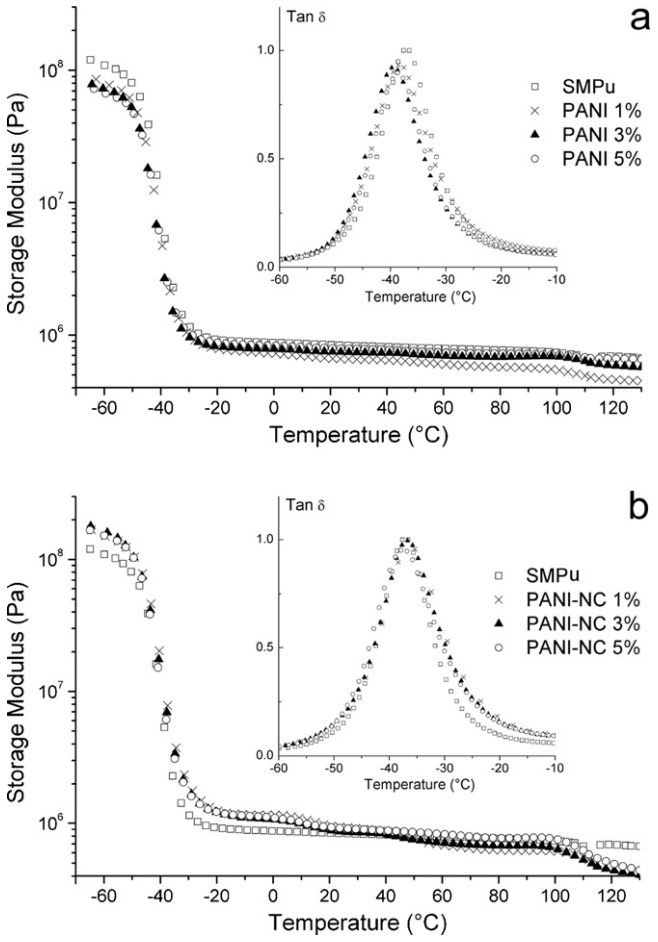

Fig. 4. Storage modulus curves and tan δ curves (inset, temperature range: −60 °C to −10 °C) of PANI (a) and PANI-NC composites (b).

samples, resulting independent from the type or concentration of nanoparticles. Events at higher temperatures could not be observed using this technique. On the other hand, rheology measurements performed on solid filmstrips confirmed these low T_g values (for the neat SMPu sample, the T_g has a value of −45.9 °C or −38.6 °C, depending if it is determined from the location of the maximum in E'' or in the tan δ curve). These measurements show another small transition at about 118 °C (Fig. 4) that appears in all the tested samples, included the polyurethane matrix. At higher temperatures, matrix and composite samples reach the flow region and the tests have to be stopped. As Fig. 4 shows, thermo-mechanical tests also reveal some minor differences between composite samples: the glass transition appears at lower temperature for both sets of composites, in comparison to that of the neat SMPu matrix, and the height of the tan δ peak decreases as filler content increases, being this effect more noticeable for PANI composites (Fig. 4a). Evidently the addition of PANI based particles to the polyurethane causes an increase in its mobility (lower T_g). Moreover, as shown in Fig. 4b, the storage modulus of polyurethane reinforced with PANI-NC samples is higher than that of the matrix, and increases as fiber concentration increases, confirming the reinforcing effect of cellulose. However, it is noticed that the increase in the storage modulus with PANI-NC concentration is only moderate in the rubbery region. Considering the relative modulus of the soft polymer matrix and the rigid cellulose, even at the low concentrations used, the modulus increase should be much higher for a nanocomposite, which indicates that the filler is acting as a classical micro-reinforcement instead of leading to a percolating network of nanoparticles. On the other hand, the storage modulus of PANI reinforced samples is lower than that of the neat SMPu in the glassy zone but reaches just about the same value in the rubbery region (Fig. 4a). Moreover, as PANI concentration increases this effect is more prominent and could be attributed to adverse interactions developed between PANI and matrix or to increasing heterogeneities in the films.

In the preparation of conductive blends of polyaniline and classical polymers the value of percolation threshold is of a crucial importance [42]. Conductive polyaniline exhibits high extinction coefficients for blue and red lights; thus, transparent films can be fabricated only at extremely low contents of the conductive phase in the blend. In addition, desired mechanical properties of the host-insulating polymer can be retained only in the case of small admixtures of polyaniline. In our case, even the samples containing 1 wt% of PANI or PANI-NC fibers are green and homogeneously colored, indicating that the transparency of the neat SMPu cannot be maintained, but also that the filler is homogeneously dispersed into the polymeric matrix, at least macroscopically. On the other hand, the surfaces of the two sets of films are quite different, as can be seen with the unaided eye: the surfaces of PANI-NC films containing up to 5 wt% filler are smooth and have metallic shine, while those containing more than 5 wt% PANI-NC and all PANI composites are rough, coarse and less shiny; these characteristics become more noticeable as PANI concentration increases, as was also noticed by other researchers in similar systems [43].

Fig. 5 shows the FESEM images of PANI and PANI-NC fibers. Particles of PANI produced by techniques of oxidative aniline polymerization in an inorganic acid water solution have a high surface tension, resulting in their tendency to aggregate, and a lowered

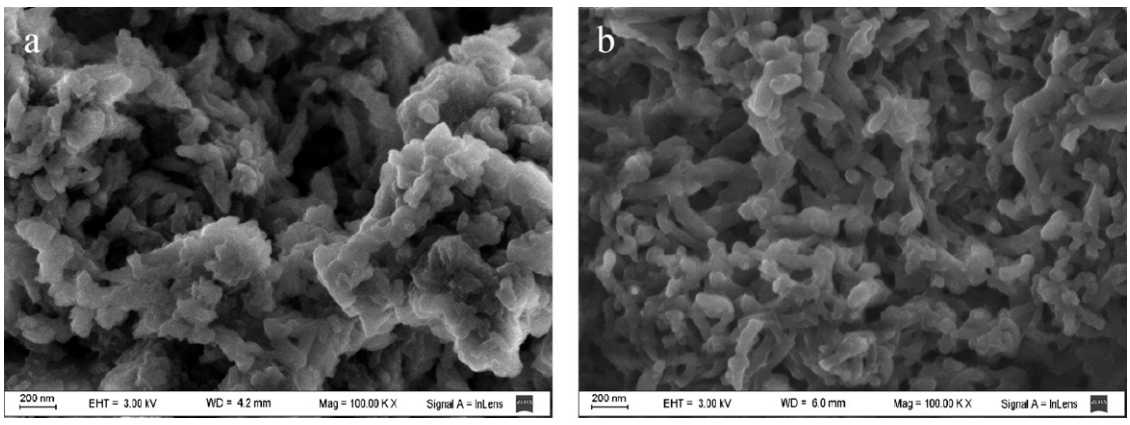

Fig. 5. FESEM images of PANI (a) and PANI-NC fibers (b).

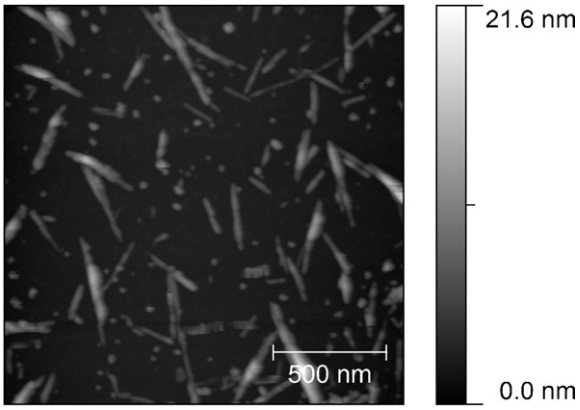

Fig. 6. AFM image of neat NC fibers.

specific surface, as indicated by other researchers [44]. After drying, large aggregates of PANI particles are formed, with sizes up to several microns, as can be noticed from FESEM pictures. As it is reported elsewhere [45,46] the basic units formed during oxidative chemical polymerization of PANI are nanofibers but due to secondary overgrowth the final product are irregularly shaped polyaniline powders. Although the sonochemical polymerization of aniline has been reported as a very good way to diminish the secondary growth [13,14], aggregation was still important in the present case.

An AFM image taken from a very diluted suspension of nanocellulose fibers in water is presented in Fig. 6. It can be noticed that individual cellulose nanofibers have an average diameter of 50 nm. However, after polymerization of aniline in the dispersed nanocellulose system, the morphology of the obtained particles is quite different from that of pure PANI (Fig. 5a). The aggregates (Fig. 5a and b) are formed by interconnected fibers with average diameters of 72 ± 14 nm for PANI nanofibers and 70 ± 10 nm for PANI-NC ones (over 20 measurements, in both cases), with larger empty space in the PANI system. Moreover, the appearance of the PANI-NC composite particles is more fibrous and well defined and they seem to have a higher aspect ratio (due to their higher length) than the PANI ones: the average length is 129 ± 24 nm for PANI nanofibers and 190 ± 44 nm for PANI-NC ones.

On the other hand, Fig. 7 shows the SEM images of the composite samples, fractured in liquid nitrogen. From the low magnification set (Fig. 7a–e), it is clear that the incorporation of any of the nanoparticles into the polyurethane matrix results in an increase of the roughness of the fractured surface, which is attributed to the increased energy dissipation during fracture. The advancing crack must change path (deflection) because of the presence of the rigid filler material, both, the PANI or the PANI–cellulose crystals (notice that the SMPu matrix is a low-modulus rubber). The higher the particle concentration, the greater the density of crack deflection sites, producing smaller and denser ripples and ridges. On the other hand, the fiber percolation threshold cannot be observed by this technique, even increasing the image magnification, as shown in Fig. 7f and g. As in other research works [20], the filled films appear containing separated white dots in SEM images, which were ascribed, as in the present case, to the nanoparticles. Even when fiber percolation through the matrix was demonstrated by other techniques in other systems [20], the special fiber arrangement that leads to continuous connection between particles was seldom noticed by microscopy observation [33]. However, the dots noticed in the SEM images appear well distributed, which is a confirmation of the success in preparing homogeneous composite SMPu films by casting from MIBK stable suspensions.

Table 1
Tensile properties of PANI and PANI-NC composites.

Property/sample	E (MPa)	σ_b (MPa)	ε_b (mm/mm)
SMPu	3.44 ± 0.24	25.5 ± 4.78	11.87 ± 0.34
1% PANI	3.65 ± 0.15	27.7 ± 2.15	11.48 ± 1.10
3% PANI	3.82 ± 0.10	18.3 ± 2.61	12.17 ± 1.54
5% PANI	4.02 ± 0.36	24.8 ± 1.10	12.47 ± 0.81
1% PANI-NC	3.53 ± 0.32	23.7 ± 5.22	13.36 ± 1.99
3% PANI-NC	3.55 ± 0.54	18.3 ± 2.66	11.42 ± 0.82
5% PANI-NC	3.96 ± 0.23	27.7 ± 2.13	11.71 ± 0.20

3.2. Mechanical properties

Table 1 summarizes the results of the tensile tests. They revealed that the addition of PANI or PANI-NC fibers increases slightly the elastic modulus (17% maximum increase for 5% PANI) and affects ultimate strength and elongation at break rather randomly. Nevertheless, the maximum deformation is very high for all the samples. According to our results, it can be concluded that the elastomeric polyurethane matrix, and not the nanofillers, controls the tensile behavior, as it was also found in other Pu based nanocomposites [33]. This conclusion is supported by the behavior shown in the stress–strain curves of the neat Pu and PANI composites (representative curves displayed in Fig. 8). It can be noticed that all the samples exhibit typical elastomeric behavior. Stress increases linearly with the strain at very small deformations (less than 3%). At higher elongations the stress–strain curve deviates considerably from the Hookean behavior, since stress is redistributed by deformation (fragmentation) and reorganization of the hard segments. Finally, the polymer cannot bear the load anymore, and the material breaks. The steep upswing of the stress–strain curve (strain hardening) can be explained by strain-induced crystallization of the SMPu soft segments [35,47].

Mechanical properties of composites or blends are profoundly influenced by their composition and morphology. It has been reported that addition of doped polyaniline to the conventional polymers above the percolation threshold impairs their mechanical properties [17] since below the percolation threshold the conducting phase is dispersed in the form of separated islands in the continuous polymeric matrix and it does not have significant influence on the macroscopic properties of the blend or composite. When the percolation threshold is reached, though, a three-dimensional network of conducting globular aggregates in the insulating matrix is created. This network is responsible for a blend being conductive, but at the same time the combination of the mechanical properties of both phases match closely the predictions of the so-called parallel model (lower limit of the combination models). From our results, it is clear that the percolation threshold for mechanical behavior was not reached, since reinforced samples perform as good or even better (elastic modulus) than the neat polyurethane. On the other hand, the absolute values of tensile properties of segmented polyurethane based composites are very dependent on the process history (solvent removal rate, thermal treatments, aging conditions, etc.); samples may exhibit differences of modulus up to 100%; the lowest resulting from plasticization by residual solvent and the highest associated with increased soft-segment crystalline content after sample storage for several days after preparation [48]. For reproducibility, all samples discussed in Table 1 and Fig. 8 were mechanically tested one month after prepared, to ensure comparable process history.

3.3. Shape memory properties

The following scenarios can be anticipated to occur during testing the sample specimens for shape memory properties [49]. First, the chains of soft segments and the fixed hard segment phase

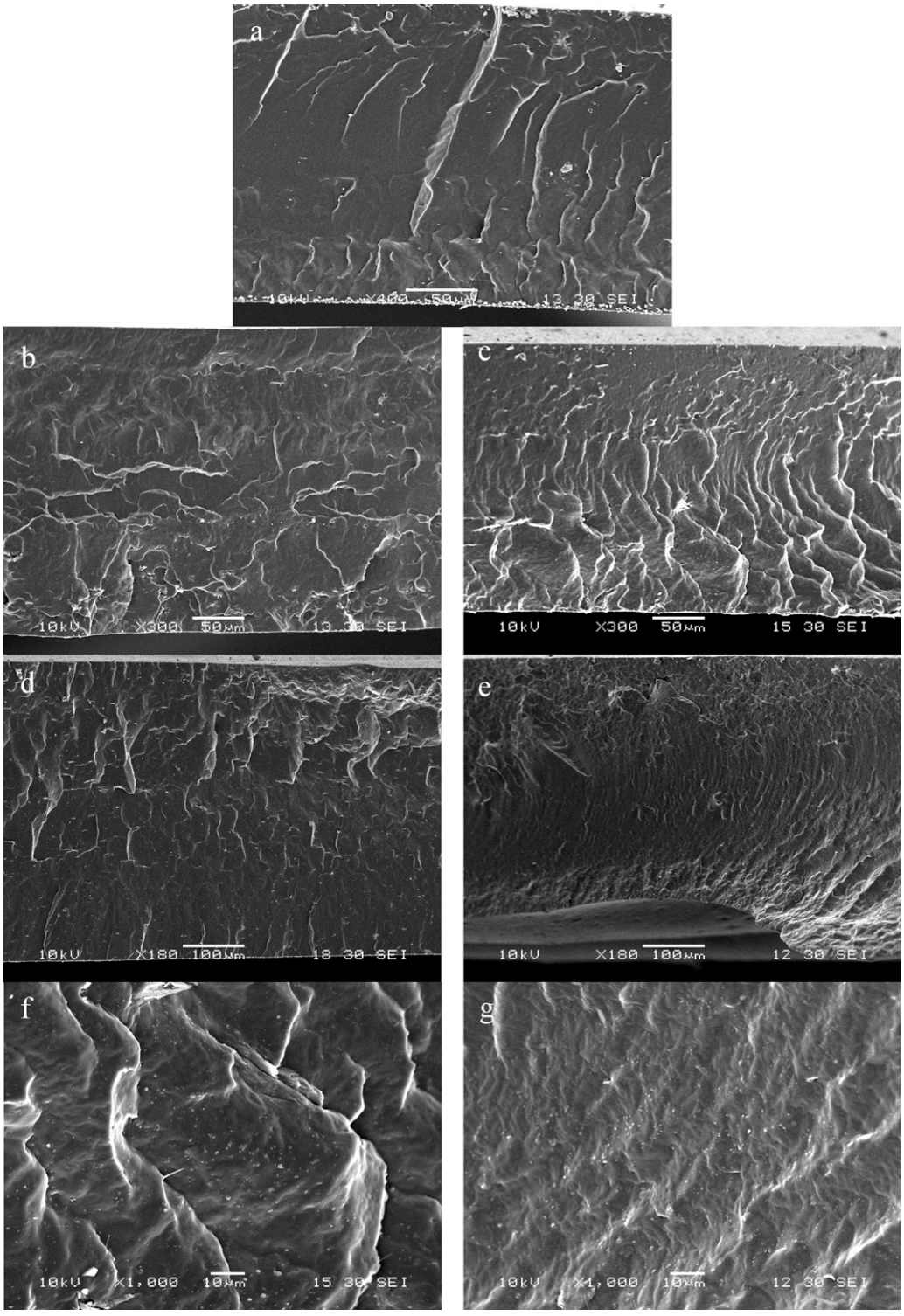

Fig. 7. SEM images of cryo-fractured composite surfaces. (a) Neat SMPu matrix; (b) PANI composite, 1 wt%; (c) PANI composite, 5 wt%; (d) PANI-NC composite, 1 wt%; (e) PANI-NC composite, 5 wt%; (f) PANI composite, 5 wt% (1000×); (g) PANI-NC composite, 5 wt% (1000×).

are oriented along the direction of stretching at room temperature. Second, the fixed hard segment phase hinders relaxation of stretched soft segment chains. Third, the soft segment crystallizes upon cooling to sub-zero temperature and provides enough restriction against relaxation of the stretched, amorphous soft segment. Therefore, the length of the sample was not anticipated to change much upon unloading; however, as the samples are not perfect shape memory materials, a small but immediate shrinkage of length occurred once the deformed sample was released. Then, by heating above the soft-segment glass transition temperature under a free load condition, the shape memory polymer could recover almost completely its initial shape, and then go through the whole process again. In this work, the cyclic procedure was repeated five times to characterize the shape memory behavior but also to check the repeatability and stability of the material.

Table 2
Shape memory properties of PANI-SMPu composites.

	Cycle #	PANI concentration (wt%)			
		0	1	3	5
R_r (%)	1	90.3 ± 2.0	91.2 ± 1.2	86.1 ± 0.6	83.7 ± 5.3
	2	92.9 ± 7.1	88.9 ± 0.6	81.9 ± 1.5	81.3 ± 8.1
	3	89.9 ± 6.6	87.6 ± 0.5	80.1 ± 0.6	79.2 ± 0.6
	4	89.9 ± 9.6	88.4 ± 1.2	78.0 ± 1.4	77.0 ± 9.2
	5	88.3 ± 10.4	86.8 ± 0.8	76.3 ± 1.8	72.2 ± 12.2
R_f (%)	1	97.1 ± 0.9	94.0 ± 0.7	98.1 ± 0.5	96.6 ± 1.4
	2	96.6 ± 0.8	96.5 ± 1.5	97.9 ± 0.6	96.7 ± 0.7
	3	94.6 ± 3.6	94.6 ± 1.6	97.8 ± 0.9	96.3 ± 0.8
	4	95.6 ± 0.8	96.1 ± 0.9	97.1 ± 0.8	96.8 ± 0.8
	5	95.6 ± 2.8	92.9 ± 3.0	97.1 ± 0.8	96.4 ± 0.6
F_r (MPa)	1	875.3 ± 112.7	937.9 ± 156.9	827.6 ± 77.8	779.3 ± 38.4
	2	846.2 ± 116.9	950.3 ± 147.7	890.7 ± 75.2	806.3 ± 15.8
	3	830.8 ± 143.8	933.0 ± 118.9	877.8 ± 34.3	792.5 ± 53.2
	4	837.3 ± 123.5	954.9 ± 110.6	925.7 ± 90.7	803.1 ± 19.1
	5	800.6 ± 81.4	937.9 ± 171.9	881.8 ± 67.5	825.3 ± 25.6

Table 3
Shape memory properties of PANI-NC-SMPu composites.

	Cycle #	PANI-NC concentration (wt%)			
		0	1	3	5
R_r (%)	1	90.3 ± 2.0	76.7 ± 12.9	81.0 ± 9.8	81.6 ± 4.4
	2	92.9 ± 7.1	69.8 ± 16.3	77.6 ± 6.8	83.2 ± 1.3
	3	89.9 ± 6.6	67.4 ± 18.6	75.1 ± 7.4	81.4 ± 3.6
	4	89.9 ± 9.6	64.8 ± 20.8	73.7 ± 8.8	80.0 ± 3.0
	5	88.3 ± 10.4	63.6 ± 20.9	68.8 ± 12.3	76.9 ± 2.0
R_f (%)	1	97.1 ± 0.9	95.2 ± 2.7	97.3 ± 0.2	97.2 ± 0.6
	2	96.6 ± 0.8	96.6 ± 1.3	97.7 ± 0.6	97.0 ± 0.8
	3	94.6 ± 3.6	96.6 ± 0.7	96.7 ± 0.9	97.1 ± 0.7
	4	95.6 ± 0.8	95.1 ± 1.9	96.7 ± 0.6	96.3 ± 1.1
	5	95.6 ± 2.8	95.0 ± 2.1	97.0 ± 0.7	96.9 ± 0.9
F_r (MPa)	1	875.3 ± 112.7	804.1 ± 40.3	932.3 ± 106.1	1027.4 ± 56.7
	2	846.2 ± 116.9	816.3 ± 16.7	893.8 ± 30.8	1116.5 ± 77.1
	3	830.8 ± 143.8	831.5 ± 48.3	897.7 ± 43.4	1066.5 ± 33.6
	4	837.3 ± 123.5	834.2 ± 60.5	831.6 ± 95.1	1054.6 ± 39.0
	5	800.6 ± 81.4	823.6 ± 39.0	935.3 ± 63.2	1086.0 ± 26.5

Tables 2 and 3 present the results of the shape memory tests. Overall, it can be noticed that both, the recovery and fixity properties are quite high, being above 60% and 94%, respectively. Although the crystallinity of the soft segments in the unstretched nanocomposites was too low to be measured by DSC, the relatively high deformation (100%) applied, as well as the low temperature used in the second part of the cycle may contribute to freeze more ordered structures of the chain molecules, which act in the shape recovery after heating [50].

Nevertheless, the stretching process induced molecular chain alignment, which is responsible for the strain hardening discussed in the tensile test and in turn, facilitated additional crystallization. Thus, stretching-induced crystallization helped the sample to fix the deformed shape, more than what was anticipated from the thermal behavior of unstretched composites reported in the previous section. Similar findings were also reported in bibliography [49]. From Tables 2 and 3 it can be noticed that the fixity and recovery of the neat polyurethane are almost not affected by cycling (within experimental error), although its recovery stress decreases as the number of cycles increases. Note that after unloading the frozen sample, the successive heating process starts while the separation between clamps (directly related to the length of the deformed sample) is held constant in the last value (ε_u) until the selected high temperature of the cycle is reached and stabilized. As the sample reaches the high temperature of the cycle, the sample tries to shrink and thus, it generates a stress measured by the universal testing machine. To keep a constant length, the machine applies the same amount of stress to balance the shrinkage stress, which is referred to as the "recovery stress". At the same time, the molecular chains recover mobility, and the material begins stress relaxation. Consequently, the recovery stress declines after reaching a maximum. A high recovery stress is associated with a low relaxation ratio [49] thus, the behavior of the neat polyurethane sample indicates that the relaxation ratio increases as the sample is cyclically deformed, possibly because the induced chain alignment during stretching improves the relaxation capacity of the samples.

On the other hand, the recovery ratio of the composites based on PANI fibers decreases with cycling, and this reduction is more evident as the amount of PANI added to the SMPu increases, while the fixity is not affect by cycling neither by PANI concentration. The recovery force of PANI composites is almost constant with cycling, however it varies with PANI concentration, showing the maximum values for 1% PANI.

Regarding PANI-NC composites, the recovery values are slightly lower than the matrix ones and a minimum at 1% PANI-NC is noticed. Moreover, the recovery capacity of these samples decreases as the number of cycle increases. As in the other cases, the fixity values are more or less independent of cycling and PANI-NC concentration. The recovery force is almost constant with cycling, but increases with PANI-NC content, although composites prepared with only 1 wt% of fibers exhibit almost the same values than the neat matrix (taking into account experimental errors), presumably because the addition of such low content of PANI-NC lead to weak points in the SMPu matrix, as reported for other similar systems

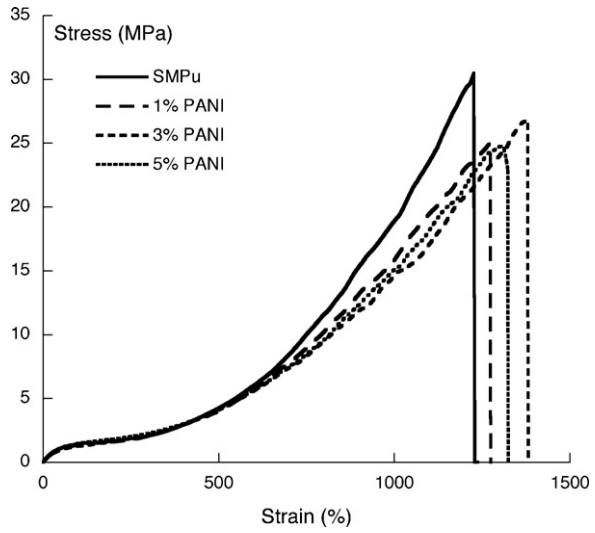

Fig. 8. Stress–strain curves of the neat SMPu and PANI composites.

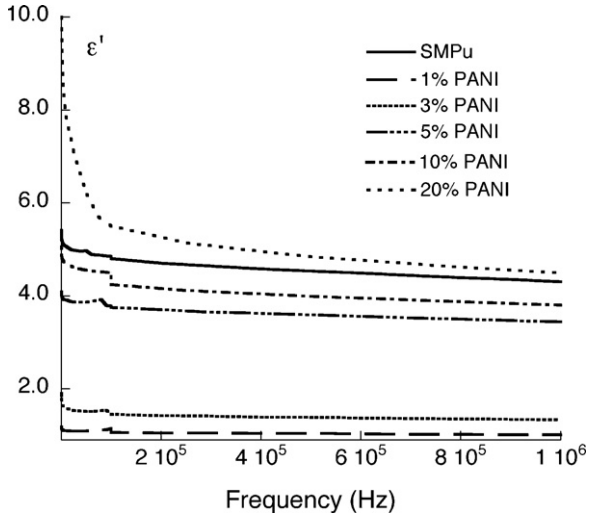

Fig. 9. Real (ε') part of complex permittivity as a function of frequency for PANI based composites.

[30]. Summarizing, the differences observed between the behavior of the neat matrix and those of the derived composites are not large, so it can be concluded that the shape memory properties of samples containing up to 5% fibers are still controlled by the polyurethane. Probably, these differences could be related to the different morphology of the PANI and PANI-NC fibers, that results in different levels of fiber–matrix interaction, affecting the induced chain alignment during stretching in different ways: not being completely erased during the recovery step of each cycle and thus, improving the soft segment crystallinity with cycling (PANI-NC samples); or improving the relaxation capacity (PANI composites).

3.4. Dielectrical properties

The ac conductivity of polyaniline is due to hopping mechanisms of charge carriers [46,51,52] that are localized around N^+ sites formed during protonation. It has been suggested that the dielectric relaxation mechanism as well as the frequency and temperature dependence of conductivity in polyaniline are due to the presence of polarons and bipolarons [53]. In the present work, the dielectrical measurements were carried out at room temperature (15 °C) and the collected data were transformed to dielectric permittivity, ε', dielectric loss factor ε'' and ac conductivity data. For this analysis, the loading of the conducting phases (PANI and PANI-NC particles) was increased up to 20 wt% in an attempt to find the electrical percolation threshold. Moreover, a sample containing only 10 wt% cellulose nanofibers (NC) was prepared and tested for the sake of comparison.

The real (ε') part of complex permittivity vs frequency for PANI and PANI-NC based composites is shown in Figs. 9 and 10, respectively. In all cases, ε' decreases as frequency increases, which confirms the polar nature of the neat SMPu (i.e. dielectric constant is frequency independent for non-polar polymers) [54]. When the frequency of the applied field is increased, the dipoles present in the system cannot reorient themselves fast enough to respond to applied electric field and as a result dielectric constant decreases [54]. As it is known, the dielectric constant of a material is a function of its capacitance, which is proportional to the quantity of the charge stored on either surface of the material in an applied electric field [55]. In case of a composite, its dielectric constant is dictated mainly by the polarity of matrix and those interfaces in subsurface (the area immediately next to the sample surfaces) of the sample [56].

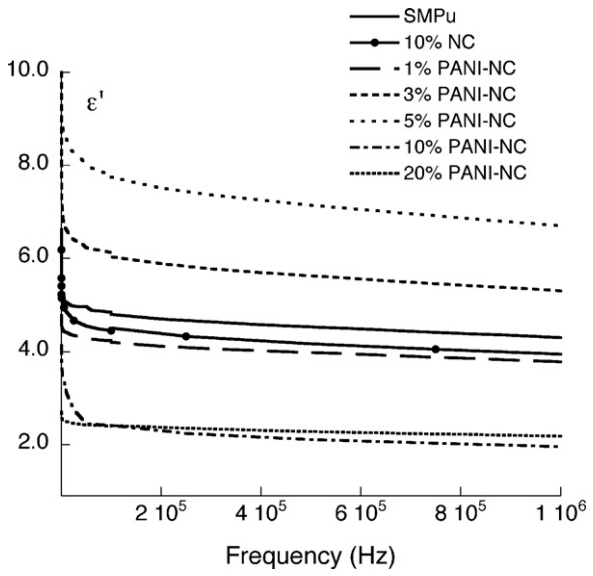

Fig. 10. Real (ε') part of complex permittivity as a function of frequency for PANI-NC and NC based composites.

Due to the important interactions developed between matrix (SMPu) and filler, some charge carriers present in PANI gets trapped and cannot freely discharge at the electrodes, which can explain up to a certain extent the decrease of the dielectric parameters with the increase of PANI concentration in the SMPu matrix, as can be noticed from Fig. 9. It can be observed that composites with 1 or 3 wt% PANI show a non-polar or a very weak polar character since ε' is almost frequency independent. As PANI concentration increased up to 5–10 wt%, the amount of charge carriers is high enough to counterbalance the effect of filler–matrix interactions and the dielectric permittivity of this sample reaches more or less the value of the neat matrix. At least 20 wt% PANI particles should be added to the SMPu to obtain a composite with higher ε' than the neat matrix. On the other hand, from Fig. 10 it can be noticed that samples containing more than 1 wt% and less than 10 wt% PANI-NC fibers display higher permittivity than the neat matrix, confirming that the interactions fiber–matrix developed when using composite filler differ in some degree from the SMPu-PANI ones. However, a further increase in the PANI-NC load led to a important reduction of the ε', probably because the dispersion of the filler into

Table 4
Electrical conductivity of bulk PANI and PANI-NC fibers.

Fiber	Frequency (Hz)	Electrical conductivity (S/m)
PANI	20	0.548
	50	0.552
	100	0.554
PANI-NC	20	2.410
	50	2.420
	100	2.430

the matrix was not as good as in the less concentrated samples, but mainly due to the roughness of the film surfaces that increases considerably respect to those of the less concentrated samples. On the other hand, the composite prepared with 10 wt% NC exhibit a dielectric permittivity slightly lower than that of the neat matrix, which is consistent with the non-conductive character of this filler. Finally, ε'' (data not shown), which is the part of the energy of an electric field that is dissipated irrecoverably as heat, is relatively low for all samples in a wide range of frequencies. At high frequencies (>10^5 Hz), ε'' increases slightly with frequency, following the trend discussed above for all samples and due to the fact that the response of the electronic, atomic and dipolar polarizable units vary with frequency [57].

The frequency dependent electrical conductivities of PANI and PANI-NC fibers are shown in Table 4. It is quite surprising to notice that composite PANI-NC fibers exhibit higher conductivity than PANI particles, but there are precedents in this respect: Sahoo et al. [58] noticed the same effect by comparing the results obtained in composites based on shape memory Pu and carbon nanotubes (MWCNT) or polypyrrole coated MWCNT, indicating that the enhancement in electrical conductivity is due to the connection of the nanotubes with numerous polypyrrole domains coated onto them. Li et al. [59] prepared PANI-coated conductive paper by in situ polymerization of aniline and confirmed that the bond between PANI and cellulose existed in the form of hydrogen bonding. Moreover, they indicated that the pulp fibers promoted the dispersion of PANI particles generated, preventing their aggregation in the reaction system, which was favorable for the doping of PANI with p-toluenesulfonic acid. Therefore, they noticed a higher doping level of the PANI in the PANI/cellulose samples than the corresponding to neat PANI particles, which was attributed to the interaction cellulose–PANI. This last explanation can be directly applied to our system, due to the manifest similarities. On the other hand, dielectric measurements confirm the success of the synthesis of conductive PANI and PANI-NC particles.

The frequency dependent electrical conductivities of selected PANI, PANI-NC and NC composite films are presented in Fig. 11. At low frequencies, the conductivity becomes almost independent of frequency, as occurred with the conductive nanofillers. All the composite films show similar behavior up to 10^5 Hz and there is not much variation in the conductivity with frequency in this range. At higher frequencies (10^5–10^6 Hz), there is an obvious increase in the conductivitiy of all the films with increasing frequency, due to the formation of excess of charge carriers [57,60]. The frequency dependence shows that the dominant conduction mechanism is the hopping of the charge carriers [61]. The polarons and bipolarons that exist in the molecular structure of PANI serve as hopping sites for the charge carriers. With the application of an electric field the localized charge carriers can hop to neighboring sites, which form a continuous network allowing the charges to travel through the entire physical dimensions of the sample and cause

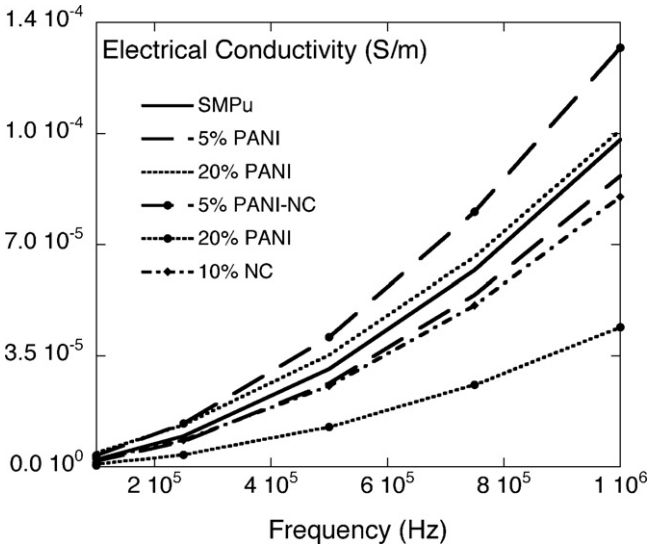

Fig. 11. Electrical conductivity of selected SMPu composites as a function of the frequency.

electrical conduction [62]. Addition of increasing contents PANI to SMPu matrix increases the number of charges participating in the relaxation process. Thus, as the amount of PANI increases, more hopping centers for charge transfer are created, and an increase in the conductivity of PANI composites should be observed. The dielectric constants of both composites increase with frequency since PANI particles are polar, therefore when a high frequency field is applied, the added conductive polymer achieve a molecular state that corresponds to polarization. According to Banerjee and Kumar [46] the frequency dependent dielectric permittivity in organic polymers like polyaniline is dominated by reorientation of molecular dipoles. However, it is noticed that the neat polyurethane matrix exhibited higher conductivity values than PANI derived composites (Fig. 11) made with up to 10% filler, in the whole frequencies range. These results indicate that PANI particles are acting more like defects instead of connected nanofibers and thus, the electrical percolation was achieved at a very high concentration (around 20 wt%). On the other hand, when PANI coated cellulose is used as reinforcement, the conductivity increases as the load increases up to 5 wt%. Higher concentrations lead to strong filler agglomeration and to the reduction of the electrical conductivity. The conductive properties of these composites depend on the molecular organization of the conductive clusters with respect to the polymer matrix [63] and on the conductive filler geometry, and filler–filler interaction. Hence, the conductivity of the PANI based composites could differ from that of the PANI-NC based samples due to the differences in the shape of the different particles, which leads to different dispersion degrees and levels of particle–particle interaction. Moreover, Pud et al. [44] indicated that the ability of PANI to form hydrogen bonds can affect the properties of the composite prepared, specially when a polymer with polar groups in its main or side chains is used as matrix; in addition, Laska [41] affirmed that if polyaniline molecules can hydrogen bond with the polymer matrix (for example, through carbonyl groups) their conformation simply follows the matrix pattern; in the other cases conformation depends only on a dopant and a solvent. The polymeric matrix used in this work contains carbonyl groups, as indicated by the band at 1728 cm^{-1} (Fig. 1) of the FTIR spectrum, and the slightly lower intensity at which the absorption bands appear in the composites confirm that filler and matrix are interacting at a certain degree.

Moreover, the differences noticed in film surfaces can also account for the different conductivity behavior, since in our test the electrical current has to flow through film thickness and thus, the electrodes are in contact with both film surfaces.

In any case, it appears that the films are in the semi conductive range, as similar composites reported in the literature [57].

4. Conclusions

Composite films based on a shape memory polyurethane and PANI or PANI-NC nanofibers were prepared by casting and MIBK evaporation. Relatively low amounts of fibers were used to prepare the composite samples with the aim of preserve the neat polyurethane attractive properties, i.e. high elongation at break.

The electrical conductivity of PANI-NC fibers resulted higher than that of the neat PANI fibers, which was explained taking into account the cellulose–PANI interactions developed during synthesis. However, the resulting composites did not achieve the conduction levels shown by the fibers and performed in the range of semi conducting materials, probably because the electrical percolation of fibers through the matrix was not reached.

Acknowledgments

The authors thank for the financial support to National Research Council of Republic Argentina (CONICET), the Science and Technology National Promotion Agency (ANPCyT) and the National University of Mar del Plata (UNMdP). The authors also thank to Hunstman Polyurethanes for supplying the SMPu.

References

[1] J.A. Malmonge, C.S. Campoli, L.F. Malmonge, D.H.F. Kanda, L.H.C. Mattoso, G.O. Chierice, Synthetic Metals 119 (2001) 87.
[2] M.R. Anderson, B.R. Mattes, H. Reiss, R.B. Kaner, Science 252 (1991) 1412.
[3] X. Wang, J. Liu, X. Huang, L. Men, M. Guo, D. Sun, Polymer Bulletin 60 (2007) 1.
[4] Y. Wang, X. Jing, Materials Science and Engineering B 138 (2007) 95.
[5] C. Dispenza, M. Leone, C.L. Presti, F. Librizzi, G. Spadaro, V. Vetri, Journal of Non-Crystalline Solids 352 (2006) 3835.
[6] P. Ghosh, S.K. Siddhanta, A. Chakrabarti, European Polymer Journal 35 (1999) 699.
[7] V. Saxena, B.D. Malhotra, Current Applied Physics 3 (2003) 293.
[8] H. Liu, J. Kameoka, D.A. Czaplewski, H.G. Craighead, Nano Letters 4 (2004) 671.
[9] S. Sukeerthi, A.Q. Contractor, Analytical Chemistry 71 (1999) 2231.
[10] J. Huang, S. Virji, B.H. Weiller, R.B. Kaner, Journal of the American Chemical Society 125 (2002) 314.
[11] J. Huang, R.B. Kaner, Angewandte Chemie International Edition 43 (2004) 5817.
[12] S.K. Pillalamarri, F.D. Blum, A.T. Tokuhiro, M.F. Bertino, Chemistry of Materials 17 (2005) 5941.
[13] X. Jing, Y. Wang, D. Wu, J. Qiang, Ultrasonics Sonochemistry 14 (2007) 75.
[14] X. Jing, Y. Wang, D. Wu, L. She, Y. Guo, Journal of Polymer Science Part A: Polymer Chemistry 44 (2006) 1014.
[15] D. Zhang, Y. Wang, Materials Science and Engineering B 134 (2006) 9.
[16] D. Li, R.B. Kaner, Chemical Communications (26) (2005) 3286.
[17] J. Laska, K. Zak, A. Proń, Synthetic Metals 84 (1997) 117.
[18] V.G. Kulkarni, Synthetic Metals 71 (1995) 2129.
[19] B.-H. Lee, H.-J. Kim, H.-S. Yang, Current Applied Physics 12 (2012) 75.
[20] N.E. Marcovich, M.L. Auad, N.E. Bellesi, S.R. Nutt, M.I. Aranguren, Journal of Materials Research 21 (2006) 870.
[21] L.H.C. Mattoso, E.S. Medeiros, D.A. Baker, J. Avloni, D.F. Wood, W.J. Orts, Journal of Nanoscience and Nanotechnology 9 (2009) 2917.
[22] O. van den Berg, M. Schroeter, J.R. Capadona, C. Weder, Journal of Materials Chemistry 17 (2007) 2746.
[23] M.L. Auad, T. Richardson, W.J. Orts, E.S. Medeiros, L.H.C. Mattoso, M.A. Mosiewicki, N.E. Marcovich, M.I. Aranguren, Polymer International 60 (2011) 743.
[24] Y. Zhu, J. Hu, K. Yeung, Acta Biomaterialia 5 (2009) 3346.
[25] C. Sivakumar, A.S. Nasar, European Polymer Journal 45 (2009) 2329.
[26] J.W. Cho, Y.C. Jung, Y.-C. Chung, B.C. Chun, Journal of Applied Polymer Science 93 (2004) 2410–2415.
[27] I. Yilgor, E. Yilgor, I.G. Guler, T.C. Ward, G.L. Wilkes, Polymer 47 (2006) 4105.
[28] J.T. Garrett, R. Xu, J. Cho, J. Runt, Polymer 44 (2003) 2711.
[29] M. Trchová, I. Šeděnková, E. Tobolková, J. Stejskal, Polymer Degradation and Stability 86 (2004) 179.
[30] T. Thanpitcha, A. Sirivat, A.M. Jamieson, R. Rujiravanit, Carbohydrate Polymers 64 (2006) 560.
[31] M.C. Arenas, E. Andablo, V.M. Castaño, Journal of Nanoscience and Nanotechnology 10 (2010) 549.
[32] S.V. Ryabov, Y.Y. Kercha, N.E. Kotel'nikova, R.L. Gaiduk, V.I. Shtompel', L.A. Kosenko, A.G. Yakovenko, L.V. Kobrina, Polymer Science Series A 43 (2001) 1256.
[33] M.L. Auad, V.S. Contos, S. Nutt, M.I. Aranguren, N.E. Marcovich, Polymer International 57 (2008) 651.
[34] R.C. Nunes, R. Pereira, J.L. Fonseca, M. Pereira, Polymer Testing 20 (2001) 707.
[35] R.M. Versteegen, R. Kleppinger, R.P. Sijbesma, E.W. Meijer, Macromolecules 39 (2005) 772.
[36] V. Sreejith, Structure and properties of processable conductive polyaniline blends, Ph.D. Thesis, National Chemical Laboratory, 2004.
[37] J. Feng, A.G. MacDiarmid, A.J. Epstein, Synthetic Metals 84 (1997) 131.
[38] Y. Xia, J.M. Wiesinger, A.G. MacDiarmid, A.J. Epstein, Chemistry of Materials 7 (1995) 443.
[39] Y. Xia, A.G. MacDiarmid, A.J. Epstein, Macromolecules 27 (1994) 7212.
[40] H. Zhang, J. Lu, X. Wang, J. Li, F. Wang, Polymer 52 (2011) 3059.
[41] J. Laska, Journal of Molecular Structure 701 (2004) 13.
[42] A. Proń, M. Zagorska, Y. Nicolau, F. Genoud, M. Nechtschein, Synthetic Metals 84 (1997) 89.
[43] W. Yin, J. Li, Y. Li, Y. Wu, T. Gu, C. Liu, Polymer International 42 (1997) 276.
[44] A. Pud, N. Ogurtsov, A. Korzhenko, G. Shapoval, Progress in Polymer Science 28 (2003) 1701.
[45] J. Huang, R.B. Kaner, Chemical Communications (4) (2006) 367.
[46] S. Banerjee, A. Kumar, The Journal of Physics and Chemistry of Solids 71 (2010) 381.
[47] M.L. Auad, M.A. Mosiewicki, T. Richardson, M.I. Aranguren, N.E. Marcovich, Journal of Applied Polymer Science 115 (2010) 1215.
[48] H. Koerner, W. Liu, M. Alexander, P. Mirau, H. Dowty, R.A. Vaia, Polymer 46 (2005) 4405.
[49] F. Cao, S.C. Jana, Polymer 48 (2007) 3790.
[50] K.K. Byung, Y.L. Sang, X. Mao, Polymer 37 (1996) 5781.
[51] M. Gosh, A. Barman, A.K. Meikap, S.K. De, S. Chatterjee, Physics Letters A 260 (1999) 138.
[52] A.N. Papathanassiou, I. Sakellis, J. Grammatikakis, E. Vitoratos, S. Sakkopoulos, E. Dalas, Synthetic Metals 142 (2004) 81.
[53] N.J. Pinto, G.P. Sinha, F.M. Aliev, Synthetic Metals 94 (1998) 199.
[54] S. Bhadra, D. Khastgir, N.K. Singha, J.H. Lee, Progress in Polymer Science 34 (2009) 783.
[55] F. Mark Herman, Encyclopedia of Polymer Science and Engineering, Dielectric Heating to Embedding, Wiley, 1986.
[56] C. Han, A. Gu, G. Liang, L. Yuan, Composites Part A: Applied Science and Manufacturing 41 (2010) 1321.
[57] S. Cetiner, H. Karakas, R. Ciobanu, M. Olariu, N.U. Kaya, C. Unsal, F. Kalaoglu, A.S. Sarac, Synthetic Metals 160 (2010) 1189.
[58] N.G. Sahoo, Y.C. Jung, H.J. Yoo, J.W. Cho, Composites Science and Technology 67 (2007) 1920.
[59] J. Li, X. Qian, L. Wang, X. An, BioResources 5 (2010) 712.
[60] T. Vishnuvardhan, V. Kulkarni, C. Basavaraja, Bulletin of Materials Science 29 (2008) 77–83.
[61] R. Singh, V. Arora, R.P. Tandon, A. Mansingh, S. Chandra, Synthetic Metals 104 (1999) 137.
[62] A.B. Afzal, M.J. Akhtar, M. Nadeem, M.M. Hassan, Current Applied Physics 10 (2010) 601.
[63] M. Tabellout, K. Fatyeyeva, P.Y. Baillif, J.F. Bardeau, A.A. Pud, Journal of Non-Crystalline Solids 351 (2005) 2835.